Charge-Assisted Hydrogen-Bonded Networks of NH₄⁺ and [Co(NH₃)₆]³⁺ with the New Linker Anion of 4-Phosphono-Biphenyl-4′-Carboxylic Acid

Christian Heering, Bahareh Nateghi and Christoph Janiak *

Institut für Anorganische Chemie und Strukturchemie, Universitätsstr*aße* 1, 40225 Düsseldorf, Germany; christian.heering@hhu.de (C.H.); bahareh.nateghi@hhu.de (B.N.)

* Correspondence: janiak@hhu.de; Tel.: +49-211-81-12286

Abstract: The new linker molecule 4-phosphono-biphenyl-4′-carboxylic acid (H_2O_3P-(C_6H_4)$_2$-COOH, H_3BPPA) has been structurally elucidated in hydrogen-bonded networks with the ammonium cation NH_4(H_2BPPA)(H_3BPPA) (**1**) and the hexaamminecobalt(III) cation [Co(NH_3)$_6$](BPPA)·$4H_2O$ (**2**). The protic O-H and N-H hydrogen atoms were found and refined in the low-temperature single-crystal X-ray structures. The hydrogen bonds in both structures are so-called charge-assisted; that is, the H-bond donor and/or acceptor carry positive and/or negative ionic charges, respectively. The H-bonded network in **1** consists of one formally mono-deprotonated 4-phosphonato-biphenyl-4′-carboxylic acid group; that is, a H_2BPPA⁻ anion and a neutral H_3BPPA molecule, which together form a 3D hydrogen-bonded network. However, an almost symmetric resonance-assisted hydrogen bond (RAHB) bond [O··· H = 1.17 (3) and 1.26 (3) Å, O···H···O = 180 (3)°] signals charge delocalization between the formal H_2BPPA⁻ anion and the formally neutral H_3BPPA molecule. Hence, the anion in **1** is better formulated as [H_2BPPA··· H··· H_2BPPA]⁻. In the H-bonded network of **2** the 4-phosphonato-biphenyl-4′-carboxylic acid is triply deprotonated, BPPA³⁻. The [Co(NH_3)$_6$]³⁺ cation is embedded between H-bond acceptor groups, –COO⁻ and –PO_3⁻ and H_2O molecules. The incorporation of sixteen H_2O molecules per unit cell makes **2** an analogue of the well-studied guanidinium sulfonate frameworks.

Keywords: hydrogen-bonded network; phosphonate-carboxylate; symmetric hydrogen bond; crystal engineering; charge-assisted H-bonds

1. Introduction

The organophosphonic acid function, which has a pK_{a1} of 2.0 for the first and a pK_{a2} of 6.59 for the second proton, is capable of forming strong metal-to-ligand coordinative bonds in thermodynamically stable complexes with high stability constants [1]. Metal organophosphonate compounds are multifunctional organic-inorganic hybrid materials and as open frameworks can be regarded in between zeolite-like [1,2] and metal-organic framework materials [3,4], whereas phosphonate metal-organic frameworks (MOFs) are considerably rarer than MOFs with carboxylate linkers, with phosphonates forming stronger bonds to metals than carboxylate groups [3]. Metal organophosphonates are stable in water or aqueous environment [5]. The use of metal phosphonates in catalysis, luminescence [6], ion or proton exchange or conductivity [7,8] and in separation is discussed and investigated [9]. Further, cobalt and iron organophosphonates are investigated for their magnetic properties [10–13]. Metal phosphonates are also promising porous materials [14,15], and can be reversibly hydrated and dehydrated [16].

Organophosphonates can contain additional functional groups such as carboxylate, hydroxyl or amino in the organo-moiety which presents a tunable functionality with a wide variety of structural motifs and properties [1,3,17]. Carboxy-phosphonates (Scheme 1) can be seen as intermediates between pure carboxylates and pure phosphonates, sharing synergies of both ligand classes. Carboxy-phosphonates can form porous or 3D metal-ligand networks [18–20]. Weng *et al.* described a 3D zinc carboxy-phosphonate, ZnPC-2, as a material for CO_2 adsorption [21].
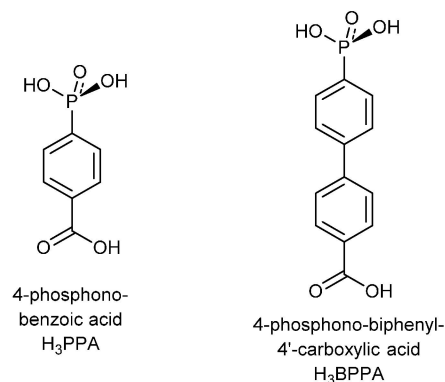

Scheme 1. Examples of phosphono-carboxylic acids.

Various metal complexes have been synthesized with a ligand from deprotonated 4-phosphono-benzoic acid, including the metals barium [22], cobalt [23], copper [23], europium [24], lead [20], lithium [25], silver [26], strontium [27], thorium [28], titanium [29], uranium [28] and zinc [30,31]. However, the extended biphenyl-based variant 4-phosphono-biphenyl-4′-carboxylic acid (H_3BPPA) was unknown so far (Scheme 1).

Herein, we present the new linker 4-phosphono-biphenyl-4′-carboxylic acid, H_3BPPA, and its deprotonated structure in hydrogen-bonded networks with NH_4^+ and $[Co(NH_3)_6]^{3+}$ cations.

2. Results and Discussion

4-Phosphono-biphenyl-4′-carboxylic acid H_3BPPA has been synthesized, following a known procedure by Merkushev *et al.* from 4-biphenyl carboxylic acid through the intermediates 4′-iodo-biphenyl-4-carboxylic acid [32] and its methyl ester, followed by the nickel(II)-catalyzed conversion to a phosphonate ester, which after hydrolysis gave H_3BPPA (Scheme 2).
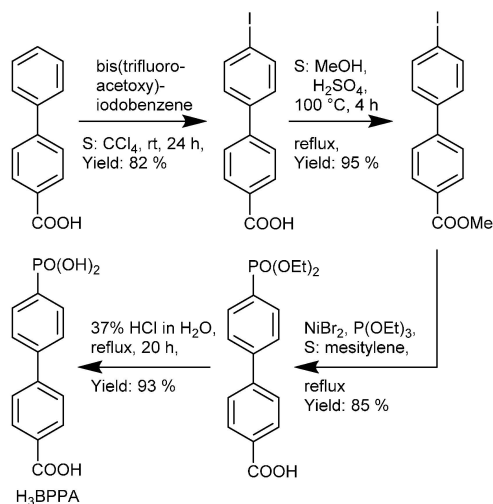
Scheme 2. Reaction sequence for the synthesis of H_3BPPA from 4-biphenyl carboxylic acid.

Neutralization of H_3BPPA with one equivalent of ammonium acetate yielded colorless crystals of formula $NH_4(HO_3P-(C_6H_4)_2-COOH)(H_2O_3P-C_6H_4-C_6H_4-COOH)$ (**1**). The ammonium monohydrogenphosphonato-biphenyl-carboxylic acid crystallized with one molecule of the free H_3BPPA acid. The best results were obtained using a 1:1 ratio, though less ammonium acetate also led to product formation of lower quality. When the neutralization of H_3BPPA was carried out with excess conc. aqueous NH_3 instead of stoichiometric ammonium acetate, the same product, **1**, was formed, albeit of lower purity. Importantly, no complete or even twofold deprotonation of H_3BPPA was achieved in that way.

The asymmetric unit of **1** consists of the ammonium-cation, and formally a H_2BPPA^- anion and a neutral H_3BPPA molecule (see below) (Figure 1a). The H_2BPPA^- anion is derived by mono-deprotonation of the phosphonic acid group. The protic O–H and N–H hydrogen atoms were found and refined with $U_{eq} = 1.5\,U_{eq}(O,N)$. The three building blocks form a three-dimensional (3D) hydrogen bonded network.

The carboxylic acid groups are oriented towards each other with the typical tail-to-tail arrangement, also known as $R_2^2(8)$-motif in the Etter-notation (Figure 1b) [33].

The biphenyl systems of the BPPA molecules are in nearly planar geometry with 0.31 (14) and 2.79 (14)° for the dihedral angles between the aryl ring planes, and 1.7 (2)° and 3.3 (2)° for the dihedral angle between −COOH and its aryl ring in the P1 and P2 molecule, respectively. The shape of the thermal ellipsoids of the carboxyl oxygen atoms O1, O2, O6, and O7 is indicative of some rotational movement (vibration) around the (carboxyl)C–C(aryl) bond (yet, no split refinement was suggested by SHELX from the principal mean square atomic displacements). Despite the presence of the biphenyl π-systems in **1**, there are no π-π interactions [34] and only few intermolecular C–H$\cdots\pi$ [35] are evident. The angle is 57° for the plane formed by one biphenyl system to its neighbor.

The ammonium cation engages all of its four (found and refined) N–H bonds in the hydrogen network to four different phosphono groups. The ammonium cations and phosphono groups form hydrogen-bonded layers parallel to the *ab*-plane, separated by the biphenyl-carboxylic acid parts (Figure 1c). Ammonium benzenephosphonate, $NH_4(HO_3PC_6H_5)$ [36], consists of a layered structure due to hydrogen bonds, with a similar motif to that of **1**.
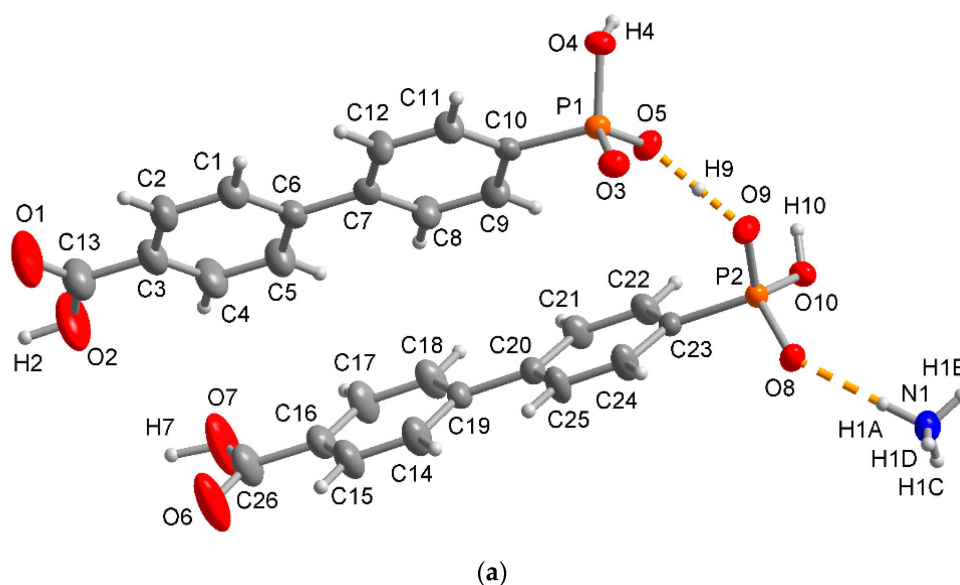

(**a**)
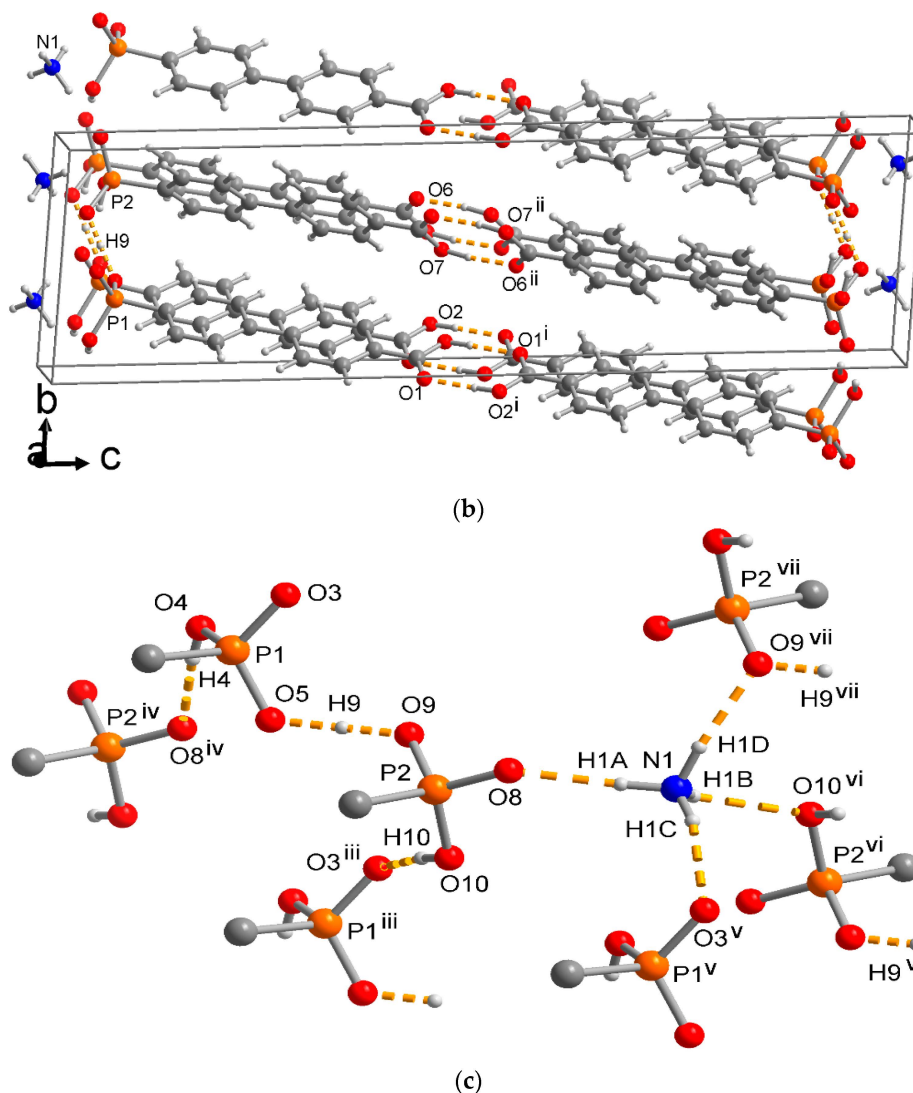
Figure 1. *Cont.*

(**b**)

(**c**)

Figure 1. (**a**) Asymmetric unit of **1** (50% thermal ellipsoids); (**b**) unit-cell packing diagram with tail-to-tail arrangement of the carboxylic acid groups (showing only the carboxyl and the O9-H-O5 H bonds for clarity); and (**c**) full hydrogen-bonding arrangement around the NH_4^+ cation and the phosphonate and phosphonic acid groups. Details of the H-bonding interactions (orange dashed lines) are given in Table 1, selected non-hydrogen bonds and angles in Table 2. Symmetry transformations: i = −1 − x, −y, 1 − z; ii = −x, 1 − y, 1 − z; iii = 1 + x, y, z; iv = x, −1 + y, z; v = 1 + x, 1 + y, z; vi = 2 − x, 2 − y, −z; vii = 1 − x, 2 − y, −z.

Table 1. Details of the hydrogen bonding interactions in **1** [a].

| D–H···A	D–H [Å]	H···A [Å]	D···A [Å]	D–H···A [°]	Symmetry Transformations
N1–H1A···O8	0.94 (3)	1.90 (3)	2.840 (3)	177 (3)	
N1–H1B···O10 vi	0.86 (3)	2.25 (3)	2.945 (3)	138 (3)	vi = 2 − x, 2 − y, −z
N1–H1C···O3 v	0.84 (3)	2.00 (3)	2.817 (3)	165 (3)	v = 1 + x, 1 + y, z
N1–H1D···O9 vii	0.95 (3)	1.92 (3)	2.845 (3)	164 (2)	vii = 1 − x, 2−y, −z
O2–H2···O1 i	0.94 (5)	1.71 (5)	2.623 (3)	164 (4)	i = −1 − x, −y, 1 − z
O4–H4···O8 iv	0.78 (3)	1.78 (3)	2.563 (2)	175 (3)	iv = x, −1 + y, z
O7–H7···O6 ii	0.99 (5)	1.66 (5)	2.642 (3)	172 (4)	ii = −x, 1 − y, 1 − z
O9–H9···O5	1.17 (3)	1.26 (3)	2.428 (2)	180 (3)	
O10–H10···O3 iii	0.83 (3)	1.72 (3)	2.537 (2)	170 (3)	iii = 1 + x, y, z

Notes: [a] D = donor, A = acceptor.

Table 2. Selected bond lengths [Å] and angles [°] in **1**.

P1–O3	1.4975 (18)	P2–O8	1.5045 (18)
P1–O5	1.5174 (18)	P2–O9	1.5190 (18)
P1–O4	1.5583 (19)	P2–O10	1.5553 (19)
P1–C10	1.787 (3)	P2–C23	1.796 (3)
C13–O1	1.235 (4)	C26–O6	1.230 (4)
C13–O2	1.283 (4)	C26–O7	1.275 (4)
O3–P1–O5	115.63 (11)	O8–P2–O9	112.38 (11)
O3–P1–O4	107.83 (10)	O8–P2–O10	109.16 (10)
O5–P1–O4	108.78 (11)	O9–P2–O10	110.04 (10)
O3–P1–C10	109.35 (11)	O8–P2–C23	109.32 (11)
O5–P1–C10	107.54 (11)	O9–P2–C23	108.76 (11)
O4–P1–C10	107.44 (11)	O10–P2–C23	107.04 (11)

Noteworthy, the H-bond O9–H9$\cdots$O5 refined to an almost symmetric O9$\cdots$H9$\cdots$O5 hydrogen bridge with very similar distances of the H atom to both oxygen neighbors (1.17 (3) and 1.26 (3) Å) and a 180 (3)° O–H$\cdots$O bond angle. This symmetric resonance-assisted hydrogen bond (RAHB) [37–41] O$\cdots$H$\cdots$O signals charge delocalization between the formal H_2BPPA^- anion (of P2) and the formally neutral H_3BPPA molecule (of P1). Hence, the anion is better formulated as $[H_2BPPA\cdots H\cdots H_2BPPA]^-$.

The interpretation of delocalized anion charge over the two phosphono groups is in agreement with the P–O bond lengths (Scheme 2). In each phosphonato group, there is a longer P–O bond of ~1.56 Å and two shorter P–O bonds between 1.50–1.52 Å. The P–O(H) bonds are 1.5583 (19) Å and 1.5553 (19) Å. One cannot clearly distinguish between a formally P=O double bond and a formally deprotonated P–O$^-$ bond. The P–O bond lengths of the symmetric O9$\cdots$H9$\cdots$O5 hydrogen bridge are only slightly longer (~1.52 Å) then what should be P=O double bonds (~1.50 Å). The negative charge is delocalized over the P–O$^-$ and P=O bonds, giving both of them a partial double bond character with P–O bond lengths between 1.50–1.52 Å (Scheme 3).
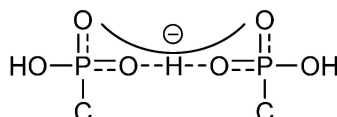
Scheme 3. Lewis valence structure for the bond order and charge-delocalization in the phosphonate groups in **1**.

Thermogravimetric analysis (TGA) of **1** shows a first a mass loss of ~4% up to 240 °C (Figure 2), which can be assigned to one molecule of ammonia (~3%), which is in agreement with literature values [42]. In a second step decarboxylation of one mol CO_2 (44 g/mol) leads to a mass loss of ~8%. With a third step of ~24% rapid dephosphonation of one mol $PO(OH)_2$ and final decarboxylation of another mol CO_2 takes place, which is followed by steady decomposition up to 700 °C.

The hydrated salt $[Co(NH_3)_6](O_3P$-$(C_6H_4)_2$-$COO)\cdot 4H_2O$, **2** could be crystallized from an aqueous ammonia solution 4-phosphono-biphenyl-4'-carboxylic acid. In a similar approach, 4-phosphono benzoic acid was crystallized with hexaaquacobalt(II) [43], and sulfonate ligands were crystallized with $[Co(NH_3)_6]^{3+}$ cations, resulting in hydrogen-bonded networks [44].

In the asymmetric unit of **2** there is one trivalent hexaamminecobalt cation, one completely deprotonated $BPPA^{3-}$ trianion and four water molecules (Figure 3a). The coordination sphere of Co^{3+} with six crystallographically different ammine ligands results in the well-known $[Co(NH_3)_6]^{3+}$ octahedron [45]. Despite its high symmetry, the $Co(NH_3)_6^{3+}$ octahedron does not reside on a special

position. The Co-N distances (Table 3) are comparable with that of $[Co(NH_3)_6]^{3+}$ in related complexes (Co-N = 1.951 (2) − 1.976 (2) Å, av. 1.956 (2) Å) [43,44,46].

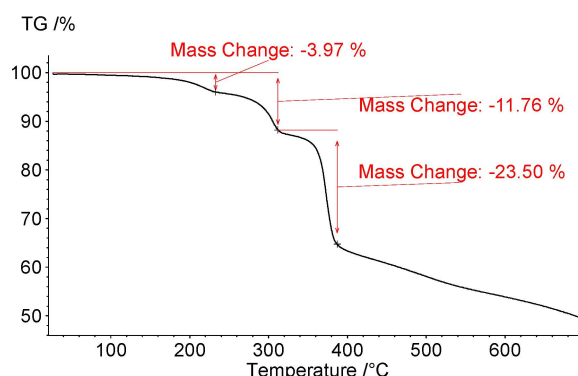**Figure 2.** Thermogravimetric analysis (TGA) of **1** in the temperature range 20–700 °C.

Again, the hydrophilic groups, $[Co(NH_3)_6]^{3+}$, –COO^-, and –PO_3^{2-}, and the crystal water molecules are arranged in slabs (parallel to the *ac* plane) with slabs of the hydrophobic biphenyl part in-between (Figure 3b,c). Such a separation of hydrophilic and hydrophobic parts of molecules is a common packing motif [47–49]. Here the hydrophilic region is organized by hydrogen bonding, the biphenyl rings are arranged by singular N–H···π, O–H···π, C–H···π or van-der-Waals interactions (see Supplementary Information). The dihedral angles within the biphenyl-carboxylate are 26.8 (4)° (ring to ring) and 42.0 (4)° (–CCOO⁻ to aryl ring).
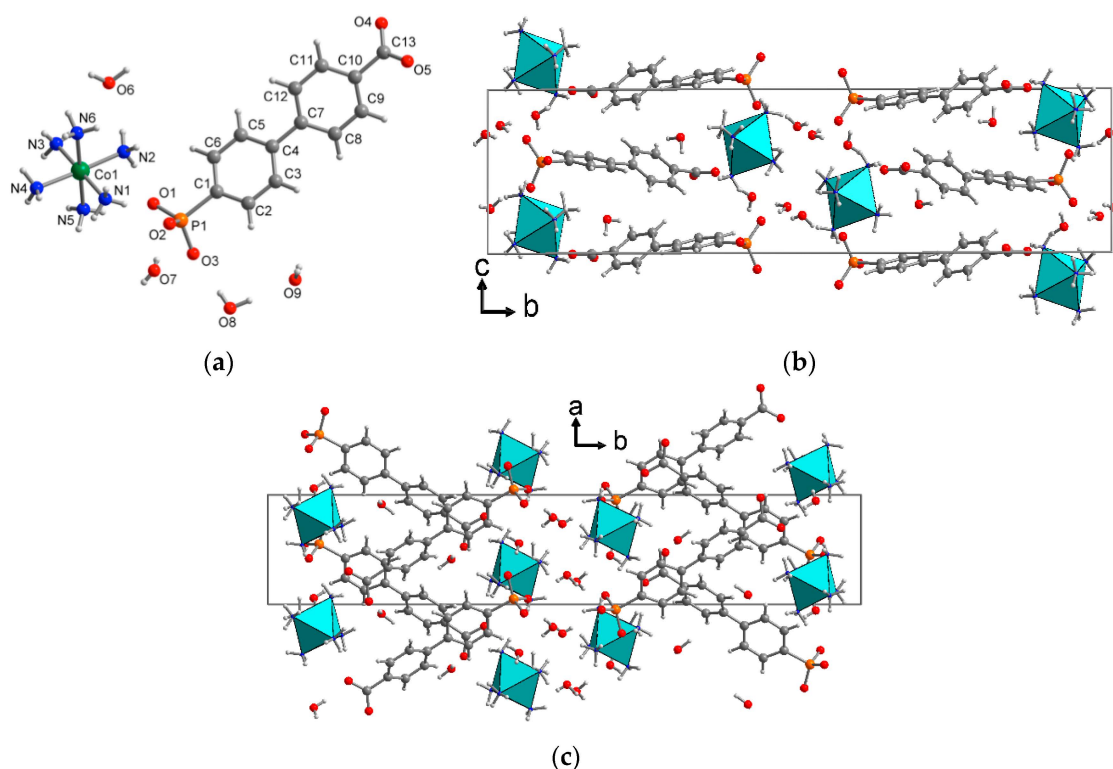

Figure 3. (**a**) Asymmetric unit of **2**; and (**b**,**c**) projections of the unit-cell packing on different planes. The $[Co(NH_3)_6]^{3+}$ cations are illustrated as octahedra; hydrogen bonds are not shown in (**a**–**c**) for clarity. Selected bond distances and angles are given in Table 3.

Table 3. Selected bond lengths and angles (Å, °) in **2**.

Co1–N1	1.957 (2)	P1–O1	1.5235 (18)
Co1–N2	1.965 (2)	P1–O2	1.5283 (18)
Co1–N3	1.951 (2)	P1–O3	1.5247 (18)
Co1–N4	1.959 (2)	P1–C1	1.820 (2)
Co1–N5	1.976 (2)		
Co1–N6	1.961 (2)		
N5–Co1–N1	87.17 (9)	N3–Co1–N4	89.51 (9)
N4–Co1–N1	91.46 (9)	N3–Co1–N2	90.46 (9)
N4–Co1–N5	90.01 (9)	N6–Co1–N1	91.82 (9)
N2–Co1–N1	88.66 (9)	N6–Co1–N5	178.81 (9)
N2–Co1–N5	92.53 (9)	N6–Co1–N2	88.07 (9)
N2–Co1–N4	177.47 (9)	N6–Co1–N3	90.31 (9)
N3–Co1–N1	177.66 (9)	N6–Co1–N4	89.40 (9)
N3–Co1–N5	90.71 (9)		

The BPPA^{3-} anions and the [Co(NH$_3$)$_6$] octahedra are connected to each other by hydrogen bonding (Table 4, Figure 4). The fully deprotonated phosphonate-carboxylate is solely an H-acceptor for the N–H and water O–H bonds. The carboxylate group is acceptor to O–H from water molecules. The four water molecules are held by hydrogen bonding from N–H and O–H-donors and –COO$^-$ and –P(O)$_2$O^{2-} acceptors.

Table 4. Details of the hydrogen bonding interactions in **2** [a].

D–H$\cdots$A	D–H [Å]	H$\cdots$A [Å]	D$\cdots$A [Å]	D–H$\cdots$A [°]	Symmetry Transformations
N1–H1A$\cdots$O8 [i]	0.84 (5)	2.71 (4)	3.327 (3)	132 (4)	i = x, y, z − 1
N1–H1B$\cdots$O2	0.84 (4)	2.14 (4)	2.976 (3)	173 (3)	
N1–H1C$\cdots$O8 [ii]	0.87 (4)	2.15 (4)	2.971 (3)	156 (3)	ii = −x + 1, −y, −z + 1
N2–H2A$\cdots$O4 [vi]	0.86 (4)	2.28 (4)	3.086 (3)	157 (3)	vi = x + 1/2, −y + 1/2, z − 1/2
N2–H2B$\cdots$O6	0.86 (4)	2.07 (4)	2.909 (4)	163 (3)	
N2–H2C$\cdots$O1	0.89 (3)	2.00 (3)	2.864 (3)	165 (3)	
N3–H3A$\cdots$O6	0.82 (5)	2.60 (5)	3.177 (4)	129 (4)	
N3–H3B$\cdots$O2 [iii]	0.90 (4)	1.90 (4)	2.791 (3)	174 (3)	iii = x + 1, y, z
N3–H3C$\cdots$O5 [viii]	0.69 (5)	2.56 (4)	3.048 (3)	130 (4)	viii = x + 3/2, −y + 1/2, z − 1/2
N3–H3C$\cdots$O4 [viii]	0.69 (5)	2.56 (4)	3.180 (3)	152 (4)	viii = x + 3/2, −y + 1/2, z − 1/2
N4–H4A$\cdots$O9 [iv]	0.90 (4)	2.05 (4)	2.937 (3)	171 (3)	iv = x + 1, y, z − 1
N4–H4B$\cdots$O7 [v]	0.83 (4)	2.77 (3)	3.270 (4)	120 (3)	v = −x + 1, −y, −z
N4–H4C$\cdots$O7 [iii]	0.86 (4)	2.00 (4)	2.852 (3)	171 (3)	iii = x + 1, y, z
N5–H5A$\cdots$O8 [ii]	0.90 (4)	2.19 (4)	3.035 (3)	157 (3)	ii = −x + 1, −y, −z + 1
N5–H5B$\cdots$O2 [iii]	0.88 (4)	2.63 (4)	3.437 (3)	153 (3)	iii = x + 1, y, z
N5–H5C$\cdots$O1	0.83 (4)	2.13 (4)	2.939 (3)	162 (3)	
N6–H6A$\cdots$O3 [i]	0.82 (4)	2.09 (5)	2.904 (3)	175 (3)	i = x, y, z − 1
N6–H6B$\cdots$O5 [viii]	0.93 (4)	2.26 (4)	3.170 (3)	167 (3)	viii = x + 3/2, −y + 1/2
N6–H6C$\cdots$O4 [vi]	0.85 (4)	2.13 (4)	2.948 (3)	160 (3)	vi = x + 1/2, −y + 1/2, z − 1/2
O6–H6E$\cdots$O5 [viii]	0.87	1.82 (1)	2.657 (4)	161 (4)	viii = x + 3/2, −y + 1/2, z − 1/2
O7–H7A$\cdots$O3 [ii]	0.62 (5)	2.12 (5)	2.740 (3)	171 (6)	ii = −x + 1, −y, −z + 1
O7–H7B$\cdots$O2	0.85 (4)	1.89 (5)	2.690 (3)	156 (4)	
O8–H8A$\cdots$O9	0.82 (5)	1.99 (5)	2.802 (3)	175 (4)	
O8–H8B$\cdots$O3	0.73 (5)	1.97 (5)	2.693 (3)	175 (5)	
O9–H9A$\cdots$O1 [vii]	0.74 (4)	1.96 (4)	2.704 (3)	176 (4)	vii = x − 1, y, z
O9–H9B$\cdots$O4 [ix]	0.78 (4)	1.95 (4)	2.728 (3)	173 (4)	ix = x + 1/2, −y + 1/2, z + 1/2

Notes: [a] D = donor, A = acceptor.

Finally, we note that in both structures, **1** and **2**, the H-bonds to the phosphonato groups are so-called charge-assisted hydrogen bonds. The hydrogen bond donor and/or acceptor carry positive and negative ionic charges, respectively, hence are usually stronger and shorter than neutral H-bonds [12,46,47,50–54]. In **1** these are bonds NH$_4^{(+)}\cdots{}^{(-)}$O-P and NH$_4^{(+)}\cdots$(H)O-P, -P-OH$\cdots{}^{(-)}$O-P (Figure 1c). In **2** these are bonds Co-NH$_3^{(+)}\cdots{}^{(-)}$O-P and HOH$\cdots{}^{(-)}$O-P (Figure 4).

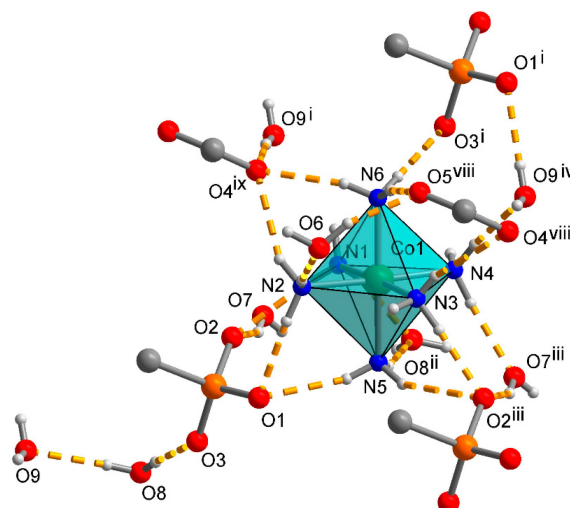**Figure 4.** Most relevant H-bonding interactions (orange dashed lines) around a $[Co(NH_3)_6]^{3+}$ cation in the structure of **2**. Details of the H-bond distances and angles are listed in Table 4. Symmetry transformations: i = x, y, z − 1; ii = −x + 1, −y, −z + 1; iii = x + 1, y, z; iv = x + 1, y, z − 1; v = −x + 1, −y, −z; vi = x + 1/2, −y + 1/2, z − 1/2; vii = x − 1, y, z; viii = x + 3/2, −y + 1/2, z − 1/2; ix = x + 1/2, −y + 1/2, z + 1/2.

The large number of hydrogen-bonds in **2** results in a thermal stability that is higher than that of other supramolecular complexes of $[Co(NH_3)_6]^{3+}$ [55,56]. The thermal stability of BPPA^{3-} is reflected by the TGA measurement (Figure 5). The mass loss in **2** up to (~17%) is due to the evaporation of the four water molecules together with one ammine ligand (17.5%). The next five ammine ligands are removed along with decarboxylation of BPPA in the range from 220 °C to 500 °C, followed by decomposition of the biphenyl system (~42% in total). The remaining mass of ~40% can be assigned to cobalt phosphonate species (~35%). It has been observed that metal phosphonates are stable up to 650 °C and higher [57].
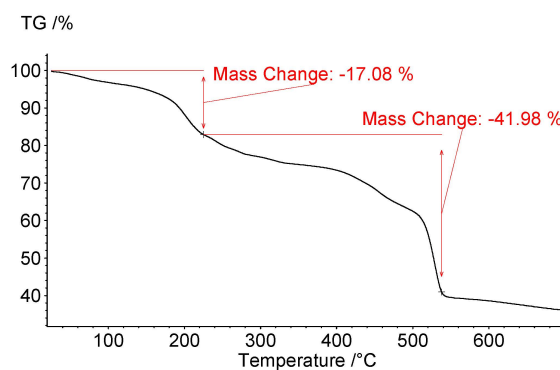

Figure 5. TGA of **2** in the temperature range 20–700 °C.

Comparison of the experimental powder X-ray diffractogram for **2** with the simulation from the single-crystal X-ray dataset (Figure 6) shows that the investigated single crystal was representative of the bulk amount when one takes into account the preferential orientation of the column- or rod-shaped crystals of **2** (Figure S1 in Supplementary Material) on the flat sample holder. Due to the preferred orientation of the rod-shaped crystals on the flat sample holder during the powder X-ray diffraction (PXRD) measurement, and their small quantity, some reflections were not present in the experimental diffraction pattern or their intensity was strongly changed. Such a behavior is discussed in detail in the literature [58–60].
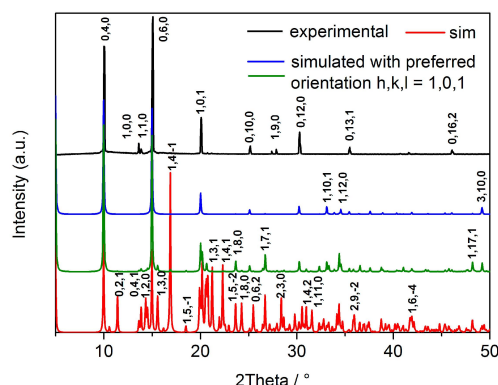
Figure 6. Comparison of the experimental PXRD pattern of **2** (**black**) with the unconstrained simulated pattern from the X-ray data (**red**) and simulated patterns with the preferred orientation of *h*, *k*, *l* = 1, 0, 1 and March–Dollase parameter = 4 (**green**) and = 10 (**blue**). The latter simulations try to take into account the rod-shaped crystal morphology of **2** with their non-random orientation on the flat sample holder. The Miller indices have been assigned to the reflections. Simulations were carried out with *Mercury* [61].

3. Materials and Methods

The chemicals used were obtained from commercial sources. No further purification has been carried out. The ligand has been synthesized starting from 4-biphenyl carboxylic acid in a four-step-synthesis. CHN analysis was performed with a Perkin Elmer CHN 2400. IR-spectra were recorded on a Bruker Tensor 37 IR spectrometer with ATR unit. Thermogravimetric analysis (TGA) was done with a Netzsch TG 209 F3 Tarsus in the range from 20 to 700 °C, equipped with Al-crucible and applying a heating rate of 10 K·min^{-1}. The melting point was determined using a Büchi Melting Point apparatus B540. For powder X-ray diffraction patterns (PXRD), a Bruker D2 Phaser powder diffractometer was used with a flat silicon, low background sample holder, at 30 kV, 10 mA for Cu-Kα radiation (λ = 1.5418 Å), with a scan speed of 0.2 s/step and a step size of 0.02° (2θ). Diffractograms were obtained on flat layer sample holders with a beam scattering protection blade installed, which led to the low relative intensities measured at 2θ < 7°. Details of the synthesis of 4-phosphono-biphenyl-4′-carboxylic acid (H$_2$O$_3$P-(C$_6$H$_4$)$_2$-COOH, H$_3$BPPA) will be given elsewhere [62].

NH$_4$(HO$_3$P-(C$_6$H$_4$)$_2$-COOH)(H$_2$O$_3$P-(C$_6$H$_4$)$_2$-COOH): In a Teflon-lined stainless steel reactor 30 mg (0.108 mmol) of H$_3$BPPA and 8.3 mg (0.108 mmol) of ammonium acetate, NH$_4$(CH$_3$COO), were suspended in 2 mL of doubly de-ionized water. Heating at 180 °C for 24 h and cooling to room temperature within 12 h led to formation of colorless crystals (Figure S1a in Supplementary Information). Yield: 29 mg (91% based on BPPA). Mp > 350 °C. Calc. for C$_{26}$H$_{25}$NO$_{10}$P$_2$ (573.43 g·mol^{-1}): C, 54.46; H, 4.39; N, 2.44%. Found: C, 53.93; H, 4.36; N, 2.02%. FT-IR (ATR) ν/cm^{-1} = 3810 (w), 3196 (w, b) 2999 (w, b), 2859 (w, b), 1672 (m), 1605 (m), 1569 (w), 1446 (m), 1248 (m), 1126 (vs), 1029 (vs), 921 (vs), 824 (vs), 763 (vs), 704 (m), 576 (s), 560 (s) (Figure S2 in Supplementary Material).

[Co(NH$_3$)$_6$](O$_3$P-(C$_6$H$_4$)$_2$-COO)·4H$_2$O: In a glass vial 9.6 mg (0.036 mmol) of [Co(NH$_3$)$_6$]Cl$_3$ and 10 mg (0.036 mmol) of 4-phosphono-biphenyl-4′-carboxylic acid were dissolved in 1.5 mL of 25% aqueous ammonia. The vial was sealed and the crystals were allowed to grow for a period of days at room temperature. After several days deep orange column-shaped crystals had grown (Figure S1b in Supplementary Material). Yield: 17 mg (91%). Mp > 350 °C. Calc. for C$_{13}$H$_{33}$CoN$_6$O$_9$P (507.34 g·mol^{-1}): C, 30.78; H, 6.56; N, 16.57%. Found: C, 30.92; H, 6.33; N, 17.12%. FT-IR (ATR) ν/cm^{-1} = 3466 (w, b), 3132 (m, b), 3051 (m, b), 2852 (w, b), 1586 (m), 1554 (m), 1528 (m), 1388 (s), 1228 (w), 1138 (m), 1100 (s), 873 (vs), 835 (m), 786 (m), 701 (m), 579 (vs) (Figure S3 in Supplementary Material).

Single Crystal X-ray Structures

Suitable crystals were carefully selected under a polarizing microscope, covered in protective oil and mounted on a 0.05 mm cryo loop. *Data collection.* Bruker Kappa APEX2 CCD X-ray diffractometer with microfocus tube, Mo-Kα radiation (λ = 0.71073 Å), multi-layer mirror system, ω- and θ-scans; data collection with APEX2, cell refinement and data reduction with SAINT [63], experimental absorption correction with SADABS [64]. *Structure analysis and refinement:* All structures were solved by direct methods using SHELXL2014; refinement of **1** was done by full-matrix least squares on F^2 using the SHELX-97 program suite [65], of **2** with OLEX 2 [66,67]. Non-hydrogen atoms were refined with anisotropic displacement parameters. Hydrogen atoms were positioned geometrically (C–H = 0.95 Å) and refined using riding models (AFIX 43 for aromatic CH with C–H = 0.93 Å and $U_{iso}(H) = 1.2U_{eq}(C)$. In **1** the protic hydrogen atoms (O–H, N–H) were found and freely refined with $U_{iso}(H) = 1.5U_{eq}$ (NH and OH).

In **2**, NH_3 hydrogen atoms were found and freely refined. Water hydrogen atoms were also found and refined, except for O6, where they were positioned geometrically (O–H = 0.870 Å) and refined using a riding model (AFIX 6) with $U_{iso}(H) = 1.5U_{eq}(O)$.

Crystal data and details on the structure refinement are given in Table 5. Graphics were drawn with DIAMOND [68]. Analyses on the supramolecular C–H···O, C–H···π and π-π-stacking interactions were done with *PLATON* for Windows [69]. CCDC 1450889 and 1450890 contain the supplementary crystallographic data for this paper. These data can be obtained free of charge via http://www.ccdc.cam.ac.uk/conts/retrieving.html.

Table 5. Crystal data and refinement details.

	1	**2**
Chemical formula	$C_{26}H_{21}O_{10}P_2 \cdot H_4N$	$C_{13}H_8O_5P \cdot CoH_{18}N_6 \cdot 4(H_2O)$
Mr	573.41	508.36
Crystal system, space group	Triclinic, P$\bar{1}$	Monoclinic, P2$_1$/n
Temperature (K)	150	173
a (Å)	5.9358(5)	7.0193(5)
b (Å)	7.5309(5)	35.454(3)
c (Å)	27.781(2)	9.2797(7)
α (°)	95.413(4)	90
β (°)	90.768(5)	111.921(4)
γ (°)	92.816(5)	90
V (Å³)	1234.65(16)	2142.4 (3)
Z	2	4
μ (mm⁻¹)	0.24	0.93
Crystal size (mm)	0.20 × 0.15 × 0.01	0.33 × 0.3 × 0.15
Absorption correction	Multi-scan, wR2(int) was 0.0937 before and 0.0571 after correction. The Ratio of minimum to maximum transmission is 0.9165. The l/2 correction factor is 0.0000.	Multi-scan, wR2(int) was 0.1520 before and 0.0844 after correction. The Ratio of minimum to maximum transmission is 0.6784. The l/2 correction factor is 0.0015.
T_{min}, T_{max}	0.683, 0.746	0.507, 0.748
No. of measured, independent and observed reflections	20157, 4937, 3104 [I > 2σ(I)]	89006, 4214, 4150 [I > 2σ(I)]
R_{int}	0.066	0.073
(sin θ/λ)max (Å⁻¹)	0.617	0.617
R[$F^2 > 2\sigma (F^2)$], wR(F^2), S	0.049, 0.121, 1.02	0.038, 0.100, 1.04
No. of reflections	4937	4214
No. of parameters	379	374
$\Delta\rho_{max}$, $\Delta\rho_{min}$ (e·Å⁻³)	0.30, −0.34	1.10, −0.85

4. Conclusions

We investigated the hydrogen-bonding potential of the new organo-phosphonate linker, H_3BPPA, in its (partially) deprotonated forms H_2BPPA^- and $BPPA^{3-}$. As expected, the protonated phosphonic acid and deprotonated phosphonate group enters into H-bonds with all of its P–O–H donors and P–O$^-$ acceptors. Remarkably and unexpectedly, an almost symmetric resonance-assisted hydrogen bond (RAHB) bond was found between the formal H_2BPPA^- anion and the formally neutral H_3BPPA molecule in **1** to give the overall anion $[H_2BPPA\cdots H\cdots H_2BPPA]^-$.

Supplementary Materials: The following are available online at http://www.mdpi.com/2073-4352/6/3/22/s001. Figure S1: Photographs of crystals of (a) $NH_4(HO_3P\text{-}(C_6H_4)_2\text{-}COOH)(H_2O_3P\text{-}(C_6H_4)_2\text{-}COOH)$, **1** and (b) $[Co(NH_3)_6](O_3P\text{-}(C_6H_4)_2\text{-}COO)\cdot 4H_2O$, **2** taken with a light microscope; Figure S2: FT-IR (ATR) spectrum of $NH_4(HO_3P\text{-}(C_6H_4)_2\text{-}COOH)(H_2O_3P\text{-}(C_6H_4)_2\text{-}COOH)$, **1**; Figure S3: FT-IR (ATR) spectrum of $[Co(NH_3)_6](O_3P\text{-}(C_6H_4)_2\text{-}COO)\cdot 4H_2O$, **2**. Figure S4: Comparison of the experimental PXRD pattern of **1** (black) with the simulated pattern from the X-ray data (red). Packing analyses.

Author Contributions: Christian Heering designed the experiments, synthesized the ligand and compound **2**. Bahareh Nateghi carried out the reaction leading to **1**. Data analysis and measurements were performed by Christian Heering, while Christoph Janiak and Christian Heering wrote the manuscript.

Conflicts of Interest: The authors declare no conflict of interest. The founding sponsors had no role in the design of the study; in the collection, analyses, or interpretation of data; in the writing of the manuscript, and in the decision to publish the results.

References

1.   Clearfield, A.; Demadis, K. *Metal Phosphonate Chemistry: From Synthesis to Applications*; Royal Society of Chemistry: Oxford, UK, 2012; pp. 45–128.

2.   Deng, M.; Liu, X.; Zheng, Q.; Chen, Z.; Fang, C.; Yue, B.; He, H. Controllable preparation and structures of two zinc phosphonocarboxylate frameworks with MER and RHO zeolitic topologies. *CrystEngComm* **2013**, *15*, 7056–7061. [CrossRef]

3.   Gagnon, K.J.; Perry, H.P.; Clearfield, A. Conventional and unconventional metal-organic frameworks based on phosphonate ligands: MOFs and UMOFs. *Chem. Rev.* **2012**, *112*, 1034–1054. [CrossRef] [PubMed]

4.   Janiak, C. Engineering coordination polymers towards applications. *Dalton Trans.* **2003**, 2781–2804. [CrossRef]

5.   Taylor, J.M.; Vaidhyanathan, R.; Iremonger, S.S.; Shimizu, G.K.H. Enhancing water stability of metal-organic frameworks via phosphonate monoester linkers. *J. Am. Chem. Soc.* **2012**, *134*, 14338–14340. [CrossRef] [PubMed]

6.   Patterson, A.R.; Schmitt, W.; Evans, R.C. Lighting-Up Two-dimensional lanthanide phosphonates: Tunable structure-property relationships towards visible and near-infrared emitters. *J. Phys. Chem. C* **2014**, *118*, 10291–10301. [CrossRef]

7.   Jiménez-García, L.; Kaltbeitzel, A.; Pisula, W.; Gutmann, J.S.; Klapper, M.; Müllen, K. Phosphonated hexaphenylbenzene: A crystalline proton conductor. *Angew. Chem. Int. Ed.* **2009**, *48*, 9951–9953. [CrossRef] [PubMed]

8.   Corma, A.; García, H.; Llabrés i Xamena, F.X. Engineering metal organic frameworks for heterogeneous catalysis. *Chem. Rev.* **2010**, *110*, 4606–4655. [CrossRef] [PubMed]

9.   Shimizu, G.K.H.; Vaidhyanathan, R.; Taylor, J.M. Phosphonate and sulfonate metal organic frameworks. *Chem. Soc. Rev.* **2009**, *38*, 1430–1449. [CrossRef] [PubMed]

10. Rojo, T.; Mesa, J.L.; Lago, J.; Bazan, B.; Pizarro, J.L.; Arriortua, M.I. Organically templated open-framework phosphite. *J. Mater. Chem.* **2009**, *19*, 3793–3818. [CrossRef]

11. Hou, S.-Z.; Cao, D.-K.; Liu, X.-G.; Li, Y.-Z.; Zheng, L.-M. Metal phosphonates based on (4-carboxypiperidyl)-*N*-methylene-phosphonate: *In situ* ligand cleavage and metamagnetism in $Co_3(O_3PCH_2\text{-}NHC_5H_9\text{-}COO)_2(O_3PCH_2\text{-}NC_5H_{10})(H_2O)$. *Dalton Trans.* **2009**, *15*, 2746–2750. [CrossRef] [PubMed]

12. Habib, H.A.; Gil-Hernández, B.; Abu-Shandi, K.; Sanchiz, J.; Janiak, C. Iron, copper and zinc ammonium-1-hydroxyalkylidene-diphosphonates with zero-, one- and two-dimensional covalent

metal-ligand structures extended into three-dimensional supramolecular networks by charge-assisted hydrogen-bonding. *Polyhedron* **2010**, *29*, 2537–2545. [CrossRef]

13. Abu-Shandi, K.; Winkler, H.; Janiak, C. Structure and mössbauer study of the first mixed-valence iron diphosphonate. *Z. Anorg. Allg. Chem.* **2006**, *632*, 629–633. [CrossRef]

14. Zhao, X.; Bell, J.G.; Tang, S.-F.; Li, L.; Thomas, K.M. Kinetic molecular sieving, thermodynamic and structural aspects of gas/vapor sorption on metal organic framework [$Ni_{1.5}(4,4'$-bipyridine$)_{1.5}(H_3L)$-$(H_2O)_3$][H_2O]$_7$ where H_6L = 2,4,6-trimethylbenzene-1,3,5-triyl tris(methylene)triphosphonic acid. *J. Mater. Chem. A* **2016**, *4*, 1353–1365. [CrossRef]

15. Zhai, F.; Zheng, Q.; Chen, Z.; Ling, Y.; Liu, X.; Weng, L.; Zhou, Y. Crystal transformation synthesis of a highly stable phosphonate MOF for selective adsorption of CO_2. *CrystEngComm* **2013**, *15*, 2040–2043. [CrossRef]

16. Kinnibrugh, T.L.; Ayi, A.A.; Bakhmutov, V.I.; Zon, J.; Clearfield, A. Reversible dehydration behavior reveals coordinatively unsaturated metal sites in microporous aluminum phosphonates. *Cryst. Growth Des.* **2013**, *13*, 2973–2981. [CrossRef]

17. Menelaou, M.; Dakanali, M.; Raptopoulou, C.P.; Drouza, C.; Lalioti, N.; Salifoglou, A. pH-Specific synthetic chemistry, and spectroscopic, structural, electrochemical and magnetic susceptibility studies in binary Ni(II)-(carboxy)phosphonate systems. *Polyhedron* **2009**, *28*, 3331–3339. [CrossRef]

18. Ling, Y.; Deng, M.; Chen, Z.; Xia, B.; Liu, X.; Yang, Y.; Zhou, Y.; Weng, L. Enhancing CO_2 adsorption of a Zn-phosphonocarboxylate framework by pore space partitions. *Chem. Commun.* **2013**, *49*, 78–80. [CrossRef] [PubMed]

19. Breeze, B.A.; Shanmugam, M.; Tuna, F.; Winpenny, R.E.P. A series of nickel phosphonate-carboxylate cages. *Chem. Commun.* **2007**, *48*, 5185–5187. [CrossRef] [PubMed]

20. Rueff, J.-M.; Perez, O.; Leclaire, A.; Couthon-Gourvès, H.; Jaffrès, P.-A. Lead(II) Hybrid Materials from 3- or 4-Phosphonobenzoic Acid. *Eur. J. Inorg. Chem.* **2009**, 4870–4876. [CrossRef]

21. Liao, T.-B.; Ling, Y.; Chen, Z.-X.; Zhou, Y.-M.; Weng, L.-H. A rutile-type porous zinc(II)-phosphonocarboxylate framework: Local proton transfer and size-selected catalysis. *Chem. Commun.* **2010**, *46*, 1100–1102. [CrossRef] [PubMed]

22. Svoboda, J.; Zima, V.; Beneš, L.; Melánová, K.; Trchová, M.; Vlček, M. New barium 4-carboxyphenylphosphonates: Synthesis, characterization and interconversions. *Solid State Sci.* **2008**, *10*, 1533–1542. [CrossRef]

23. Pütz, A.-M.; Carrella, L.M.; Rentschler, E. A distorted honeycomb motive in divalent transition metal compounds based on 4-Phosphonbenzoic acid and exchange coupled Co(II) and Cu(II): Synthesis, structural description and magnetic properties. *Dalton Trans.* **2013**, *42*, 16194–16199. [CrossRef] [PubMed]

24. Rueff, J.-M.; Barrier, N.; Boudin, S.; Dorcet, V.; Caignaert, V.; Boullay, P.; Hix, G.B.; Jaffrès, P.-A. Remarkable thermal stability of Eu(4-phosphonobenzoate): Structure investigations and luminescence properties. *Dalton Trans.* **2009**, *47*, 10614–10620. [CrossRef] [PubMed]

25. Li, J.-T.; Guo, L.-R.; Shen, Y.; Zheng, L.-M. LiF-assisted crystallization of zinc 4-carboxyphenylphosphonates with pillared layered structures. *CrystEngComm* **2009**, *11*, 1674–1678. [CrossRef]

26. Rueff, J.-M.; Perez, O.; Caignaert, V.; Hix, G.; Berchel, M.; Quentel, F.; Jaffrès, P.-A. Silver-based hybrid materials from meta- or para-phosphonobenzoic acid: Influence of the topology on silver release in water. *Inorg. Chem.* **2015**, *54*, 2152–2159. [CrossRef] [PubMed]

27. Zima, V.; Svoboda, J.; Beneš, L.; Melánová, K.; Trchová, M.; Dybal, J. Synthesis and characterization of new strontium 4-carboxyphenylphosphonates. *J. Solid State Chem.* **2007**, *180*, 929–939. [CrossRef]

28. Adelani, P.O.; Albrecht-Schmitt, T.E. Comparison of thorium (IV) and uranium (VI) carboxyphosphonates. *Inorg. Chem.* **2010**, *49*, 5701–5705. [CrossRef] [PubMed]

29. Melánová, K.; Klevcov, J.; Beneš, L.; Svoboda, J.; Zima, V. New layered functionalized titanium (IV) phenylphosphonates. *J. Phys. Chem. Solids* **2012**, *73*, 1452–1455. [CrossRef]

30. Li, J.-T.; Cao, D.-K.; Akutagawa, T.; Zheng, L.M. $Zn_3(4$-$OOCC_6H_4PO_3)_2$: A polar metal phosphonate with pillared layered structure showing SHG-activity and large dielectric anisotropy. *Dalton Trans.* **2010**, *39*, 8606–8608. [CrossRef] [PubMed]

31. Chen, Z.; Zhou, Y.; Weng, L.; Zhao, D. Mixed-solvothermal syntheses and structures of six new zinc phosphonocarboxylates with zeolite-type and pillar-layered frameworks. *Cryst. Growth Des.* **2008**, *8*, 4045–4053. [CrossRef]

32. Merkushev, E.B.; Shvartzberg, M.S. *Organoiodine Compounds and Syntheses Based on Them*; Tomsk Gos. Pedagogicheskii Institut: Tomsk, Soviet Union, 1982; pp. 2598–2601.

33. Etter, M.C. Encoding and decoding hydrogen-bond patterns of organic compounds. *Acc. Chem. Res.* **1990**, *23*, 120–126. [CrossRef]

34. Janiak, C. A critical account on π–π stacking in metal complexes with aromatic nitrogen-containing ligands. *J. Chem. Soc. Dalton Trans.* **2000**, *21*, 3885–3896. [CrossRef]

35. Nishio, M. CH/π hydrogen bonds in crystals. *CrystEngComm* **2004**, *6*, 130–158. [CrossRef]

36. Lin, Z.; Lei, X.-Q.; Bai, S.-D.; Ng, S.W. Ammonium benzenephosphonate. *Acta Crystallogr. Sect. E.—Struct Rep. Online* **2008**, *64*, o1607. [CrossRef] [PubMed]

37. Gilli, G.; Gilli, P. *On Noncovalent Interactions in Crystals: Supramolecular Chemistry: From Molecules to Nanomaterials*; Steed, J., Gale, P.A., Eds.; Wiley: Chichester, UK, 2012; Volume 6, pp. 2829–2868.

38. Góra, R.W.; Maj, M.; Grabowski, S.J. Resonance-assisted hydrogen bonds revisited. Resonance stabilization *vs.* charge delocalization. *Phys. Chem. Chem. Phys.* **2013**, *15*, 2514–2522. [CrossRef] [PubMed]

39. Sanz, P.; Mó, O.; Yáñez, M.; Elguero, J. Resonance-assisted hydrogen bonds: A critical examination. structure and stability of the enols of β-diketones and β-enaminones. *J. Phys. Chem. A* **2007**, *111*, 3585–3591. [CrossRef] [PubMed]

40. Gilli, P.; Bertolasi, V.; Pretto, L.; Ferretti, V.; Gilli, G. Covalent *versus* electrostatic nature of the strong hydrogen bond: Discrimination among single, double, and asymmetric single-well hydrogen bonds by variable-temperature X-ray crystallographic methods in β-diketone enol RAHB systems. *J. Am. Chem. Soc.* **2004**, *126*, 3845–3855. [CrossRef] [PubMed]

41. Gilli, P.; Bertolasi, V.; Ferretti, V.; Gilli, G. Evidence for intramolecular N–H···O resonance-assisted hydrogen bonding in enaminones and related heterodienes. A combined crystal-structural, IR and NMR spectroscopic, and quantum-mechanical investigation. *J. Am. Chem. Soc.* **2000**, *122*, 10405–10417. [CrossRef]

42. Feng, C.; Liang, M.; Jiang, J.; Huang, J.; Liu, H. Synergistic effect of a Novel triazine Charring Agent and ammonium polyphosphate on the flame retardant properties of Halogen-Free Flame Retardant Polypropylene composites. *Thermochim. Acta* **2016**. [CrossRef]

43. Wilk, M.; Janczak, J.; Videnova-Adrabinska, V. Hexaaquacobalt(II) bis[hydrogen bis(4-carboxyphenyl-phosphonate)] dihydrate. *Acta Crystallogr. Sect. C—Cryst. Struct. Commun.* **2011**, *67*, 9–12. [CrossRef] [PubMed]

44. Wang, X.-Y.; Justice, R.; Sevov, S.C. Hydrogen-bonded metal-complex sulfonate (MCS) inclusion compounds: Effect of the guest molecule on the host framework. *Inorg. Chem.* **2007**, *46*, 4626–4631. [CrossRef] [PubMed]

45. Morral, F.R. Alfred werner and cobalt complexes. *Adv. Chem.* **2009**, *6*, 70–77.

46. Reddy, D.S.; Duncan, S.; Shimizu, G.K.H. A Family of supramolecular inclusion solids based upon second-sphere interactions. *Angew. Chem. Int. Ed.* **2003**, *42*, 1360–1364. [CrossRef] [PubMed]

47. Dorn, T.; Chamayou, A.-C.; Janiak, C. Hydrophilic interior between hydrophobic regions in inverse bilayer structures of cation–1,1′-binaphthalene- 2,2′-diyl phosphate salts. *New J. Chem.* **2006**, *30*, 156–167. [CrossRef]

48. Maclaren, J.K.; Sanchiz, J.; Gili, P.; Janiak, C. Hydrophobic-exterior layer structures and magnetic properties of trinuclear copper complexes with chiral amino alcoholate ligands. *New J. Chem.* **2012**, *36*, 1596–1609. [CrossRef]

49. Enamullah, M.; Vasylyeva, V.; Janiak, C. Chirality at metal and helical ligand folding in optical isomers of chiral bis(naphthaldiminato)nickel(II) complexes. *Inorg. Chim. Acta* **2013**, *408*, 109–119. [CrossRef]

50. Ward, M.D. Design of crystalline molecular networks with charge-assisted hydrogen bonds. *Chem. Commun.* **2005**, *47*, 5838–5842. [CrossRef] [PubMed]

51. Gil-Hernández, B.; Maclaren, J.K.; Höppe, H.A.; Pasan, J.; Sanchiz, J.; Janiak, C. Homochiral lanthanoid(III) mesoxalate metal-organic frameworks: Synthesis, crystal growth, chirality, magnetic and luminescent properties. *CrystEngComm* **2012**, *14*, 2635–2644. [CrossRef]

52. Maclaren, J.K.; Janiak, C. Amino-acid based coordination polymers. *Inorg. Chim. Acta* **2012**, *389*, 183–190.

53. Chamayou, A.-C.; Neelakantan, M.A.; Thalamuthu, S.; Janiak, C. The first vitamin B6 zinc complex, pyridoxinato-zinc acetate: A 1D coordination polymer with polar packing through strong inter-chain hydrogen bonding. *Inorg. Chim. Acta* **2011**, *365*, 447–450. [CrossRef]

54. Drašković, B.M.; Bogdanović, G.A.; Neelakantan, M.A.; Chamayou, A.-C.; Thalamuthu, S.; Avadhut, Y.S.; Schmedt auf der Günne, J.; Banerjee, S.; Janiak, C. *N-o*-Vanillylidene-L-histidine: Experimental charge density

analysis of a double zwitterionic amino acid Schiff-base compound. *Cryst. Growth Des.* **2010**, *10*, 1665–1676. [CrossRef]

55. Collins, L.W.; Wendlandt, W.W.; Gibson, E.K. The thermal dissociation of the $[Co(NH_3)_5Cl]Cl_2$ and $[Co(NH_3)_5Br]Br_2$ complexes in vacuo. *Thermochim. Acta* **1974**, *8*, 303–306. [CrossRef]

56. Saito, A. Thermal decomposition of the complexes $[Co(NH_3)_6][Nd(SO_4)_3] \cdot nH_2O$. *Thermochim. Acta* **1986**, *102*, 373–386. [CrossRef]

57. Dines, M.B.; DiGiacomo, P.M. Derivatized lamellar phosphates and phosphonates of M(IV) ions. *Inorg. Chem.* **1981**, *20*, 92–97. [CrossRef]

58. Mittemeijer, E.J.; Welzel, U. *Modern Diffraction Methods*; Wiley: Weinheim, Germany, 2013.

59. Pecharsky, V.; Zavalij, P. *Fundamentals of Powder Diffraction and Structural Characterization of Materials*, 2nd ed.; Springer: New York, NY, USA, 2008.

60. Dollase, W.A. Correction of intensities for preferred orientation in powder diffractometry: Application of the March model. *J. Appl. Cryst.* **1986**, *19*, 267–272. [CrossRef]

61. Macrae, C.F.; Edgington, P.R.; McCabe, P.; Pidcock, E.; Shields, G.P.; Taylor, R.; Towler, M.; van de Streek, J. Mercury: Visualization and analysis of crystal structures. *J. Appl. Cryst.* **2006**, *39*, 453–457. [CrossRef]

62. Heering, C.; Francis, B.; Nateghi, B.; Makhloufi, G.; Janiak, C. Syntheses, structures and properties of group 12 element (Zn, Cd, Hg) coordination polymers with a phosphonate-biphenyl-carboxylate linker. *CrystEngComm* **2016**. (to be submitted).

63. APEX2. *SAINT, Data Reduction and Frame Integration Program for the CCD Area-Detector System, Bruker Analytical X-ray Systems*; Data Collection program for the CCD Area-Detector System: Madison, WI, USA, 1997–2006.

64. Sheldrick, G. *SADABS: Area-Detector Absorption Correction*; University of Göttingen: Göttingen, Germany, 1996.

65. Hübschle, C.B.; Sheldrick, G.M.; Dittrich, B. ShelXle: A graphical user interface for SHELXL. *J. Appl. Cryst.* **2011**, *44*, 1281–1284. [CrossRef] [PubMed]

66. Bourhis, L.J.; Dolomanov, O.V.; Gildea, R.J.; Howard, J.A.K.; Puschmann, H. The anatomy of a comprehensive constrained, restrained refinement program for the modern computing environment—*Olex2* dissected. *Acta Crystallogr. Sect. A* **2015**, *71*, 59–75. [CrossRef] [PubMed]

67. Dolomanov, O.V.; Bourhis, L.J.; Gildea, R.J.; Howard, J.A.K.; Puschmann, H. *OLEX2*: A complete structure solution, refinement and analysis program. *J. Appl. Cryst.* **2009**, *42*, 339–341. [CrossRef]

68. Brandenburg, K. *DIAMOND*; version 3.2; Crystal and Molecular Structure Visualization; Crystal Impact—K. Brandenburg & H. Putz Gbr: Bonn, Germany, 2009.

69. Spek, A.L. Structure validation in chemical crystallography. *Acta Crystallogr. Sect. D—Biol. Crystallogr.* **2009**, *65*, 148–155. [CrossRef] [PubMed]